Ideal fluid flow past obstacles in an arbitrary channel: comparison of numerical and experimental results

By R. WEBER AND J. HUREAU

Laboratoire de Mécanique et d'Énergétique, École Supérieure de l'Énergie et des Matériaux,
Université d'Orléans, 8, Rue Léonard de Vinci, 45072 Orléans Cedex 2, France

This paper analyses a numerical model of a flow around an obstacle bounded in a channel with arbitrary walls. The model is based on the usual two-dimensional model of ideal incompressible weightless fluid. It is validated here by comparison with analytical findings and experimental data, which consisted of the velocity field determined by particle image velocimetry (PIV). Despite the simplicity of our wake model, the numerical data are usually in good agreement with the analytical and experimental data.

1. Introduction

In aerodynamics and hydrodynamics, a wake is considered to be an area of disturbed fluid behind an obstacle in a flow. It may be thin or thick, and is analysed differently in each case. That is, a thin wake usually occurs when the obstacle (e.g. an airfoil) is thin and at low incidence, and the problem is then generally solved by Joukowski's theory, whereas a thick wake occurs when the boundary layer separates on the obstacle, as it will with thick obstacles, profiles at high incidence, obstacles with edges, and blunt bodies. A jet is similar to a thick wake in that it consists of one fluid flowing around another steadier one, as explained by Birkhoff & Zarantonello (1957) and others, so that the same method can be used to solve thick wake problems and jet problems.

As early as 1868, Helmholtz and Kirchhoff set up the classical two-dimensional theory of jets and thick wakes in which the flow is considered to be irrotational and steady, the fluid to be ideal, incompressible, and weightless, and the wake an infinite dead zone. Many flow configurations have been studied with this theory, some without checking any of the restrictive hypotheses beforehand (such as the incompressibility or weight of the fluid).

The flow configurations first studied were very simple: the flow is bounded by free streamlines (jets) and/or rigid planar or circular walls (obstacles or channels). Examples of these classical configurations, which are usually not very realistic because of the geometry, can be found in the monographs of Birkhoff & Zarantonello (1957), Jacob (1959), Gurevich (1966) or Milne-Thomson (1968).

The approach used for solving them is based on conformal mapping by the Schwarz–Christoffel formula (flow domain mapped onto a half-plane) and the Joukowski or the Lévi–Civita method (mapping onto a half-unit disk). With advances in computer science, authors have recently been able to consider more realistic,

complicated problems with curved walls. One numerical method developed by Bloor (1978) is based on a generalization of the Schwarz–Christoffel formula and requires equations for the walls. This has been used to study free-surface flows over arbitrary topography with gravity (King & Bloor 1987, 1990), and an ideal fluid jet impinging on an uneven wall (Peng & Parker 1997), for example. Another method, introduced by Elcrat & Trefethen (1986), uses a modified Schwarz–Christoffel formula. This is restricted to polygonal bounded flows (Dias & Elcrat 1992). Birkhoff & Zarantonello introduced the third and most widely used method, in which gravity is sometimes considered, but the wall geometries used are usually simple (arc of a circle or polygonal). Examples of this can be found in Vanden-Broeck & Keller (1982) for jets rising and falling under gravity; in Forbes & Schwarz (1982) and Hanna, Abdel-Malek & Abd-el-Malek (1996) for free-surface flows over semicircular or trapezoidal obstacles; and in Dias & Tuck (1991) for weir flows and waterfalls. A fourth numerical method – the one we use in this paper – was then developed for two-dimensional flows. With this method, no conditions are placed on the solid boundaries. The configurations that can be treated are more general because the wall geometry can be uneven and no equations are needed for them (Hureau, Brunon & Legallais 1996 and Hureau & Weber 1998 for example), and gravity can be considered too (Toison & Hureau 2000).

In these studies, the wake model used is the classical one introduced by Helmholtz. It considers a dead flow area extending to infinity behind the obstacle where the velocity is zero and the pressure (P_0) is the same as the free-stream pressure (P_∞) far ahead of the obstacle, i.e. $P_0 = P_\infty$. It is well known by comparison with experimental results that the drag of obstacles in infinite streams is poorly evaluated using this model. So finite thick wakes were modelled differently. The first such model, developed Cisotti (1911), could not predict other than zero drag. In order to be able to change the pressure in the dead flow area behind the obstacle, Riabouchinsky (1921) then considered a mirror obstacle. This method could be used only with zero-lift obstacles, so its application was limited in practice. A third method, introduced by Efros (1946), considers a part of the re-entering jet flowing around the obstacle. But to predict better drag forces for the lifting systems, the Helmholtz method was finally reconsidered. Eppler (1954), Roskho (1954), and later Wu & Wang (1964) studied a two-part dissipative wake model in which the wake just behind the obstacle is a dead-flow area at some pressure P_0 other than free stream ($P_0 \neq P_\infty$), and this is extended in a horizontal strip downstream where the pressure gradually returns to P_∞. To obtain good results, the pressure P_0 has to be determined by experiment. A modification of the wake hypothesis by Joukowski and later analysed by Roskho (1954), Eppler (1954), and Legallais, Hureau & Brunon (1995) lead them to introduce the 'virtual wall model'. In this model, the wake is delimited by two virtual planes enclosing a wake at a pressure P_0 other than the free-stream pressure P_∞. In this way, the drag is predicted more exactly.

In this paper, we will consider the flow around an arbitrary obstacle placed in an uneven channel (figure 1). Our wake model is close to that of Helmholtz because the pressures in the wake and in the flow behind the obstacle are the same (P_∞); but they are different from the free-stream pressure ahead of the obstacle (P_{∞_A}) because of the presence of the channel. This paper generalizes the numerical process developed by Birkhoff & Zarantonello (1957), Gurevich (1966) and others, and which has hitherto been applied only to very simple symmetrical configurations (planar, horizontal walls, with obstacles limited to plates, symmetrical wedges, or arcs of a circle). We consider general obstacle geometries with uneven walls, to see if the general problem of the
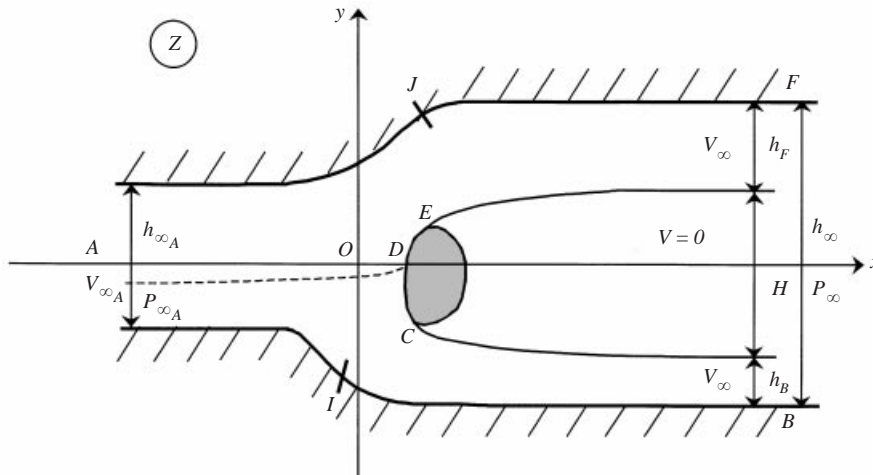
FIGURE 1. Obstacle in a channel. Notation.

flow past an obstacle in a channel is completely solved under the general ideal fluid assumption and the wake model used. Previous numerical and experimental results (Weber *et al.* 1999) concerning another flow configuration have shown that numerical and experimental data compare better if the wake is not very large, in spite of the wake simplicity. So, since the flow is bounded (P_∞ is not the same as P_{∞_A}), the drag evaluation should also be better.

Our aim in this study was to compare our numerical data with experimental data to see if this kind of numerical treatment of the problem could yield a good approximation of the steady flow around the obstacle and its wake, and of the pressure distribution on the obstacle. Our wake model is simplified, of course, but the results are reasonable and are obtained quickly. The problem of the unsteady wake is not studied here. The Brillouin condition (see § 2.5) is not used, but we needed to know the position of the two separation points on the obstacle. This is done by experiment, for the time being, using particle image velocimetry (PIV) and pressure probes. As the comparison between experimental and numerical data is sufficiently good, it will be possible, in the future, to predict these positions by coupling the method with a boundary layer model.

2. Solution

The numerical study consists in determining the geometry of the free streamlines behind an obstacle placed in a flow bounded by an arbitrary channel. The velocity in the flow field and the widths of the flow at the exit of the channel will be determined. The usual two-dimensional flow theory for ideal incompressible weightless fluid is used to solve the problem.

2.1. *Problem formulation*

Let an arbitrary obstacle of known geometry be placed in a flow bounded by arbitrary walls (figure 1). The wetted wall of the obstacle is denoted CDE, in which D is the dividing point of the flow, and C and E its separation points (positions assumed to be known). The wetted arclength is L_{Obs}. The wall below the obstacle is denoted AB, and the wall above AF. The walls are assumed to be parallel far from the obstacle,
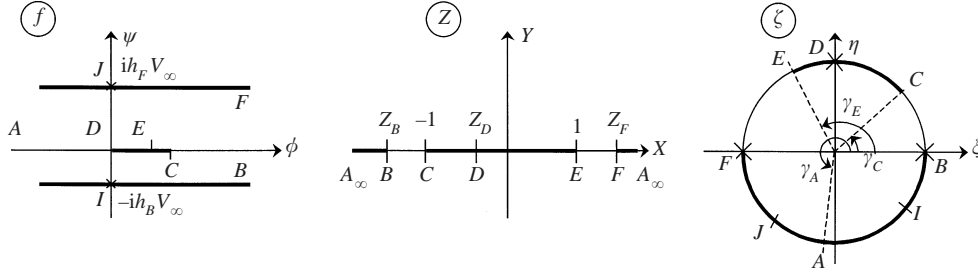
FIGURE 2. Mapping planes.

and their direction defines the *x*-axis of Cartesian coordinates. The geometry of all the solid boundaries (obstacle and channel) are known in this Cartesian coordinate system. Let h_A, P_{∞_A}, and V_{∞_A} be the channel width and the flow pressure and velocity at the infinite point A, respectively. The obstacle divides the channel exit flow into two fluid jets whose widths are denoted h_B and h_F. B and F represent the same point at the exit of the channel at infinity; however, to avoid any ambiguity in the theoretical development of the method, we decided to differentiate between infinite upper and lower streams. The pressure and the velocity, denoted P_∞ and V_∞, respectively, are taken to be equal at these two points B and F. The channel width behind the wall is denoted h_∞.

In the whole fluid flow domain, described by the complex position z, the function w, representing the complex velocity ($w = \mathrm{d}f/\mathrm{d}z$ with f the complex potential of the flow), has to satisfy the boundary conditions

$$\lim_{z \to A} w(z) = V_{\infty_A}, \tag{2.1}$$

$$\lim_{z \to B,F} w(z) = V_\infty, \tag{2.2}$$

$$\mathrm{Im}\{w(z)\mathrm{d}z\} = 0 \quad \text{on the wetted walls } CDE, \ AB \text{ and } AF, \tag{2.3}$$

the Bernoulli equation

$$P_{\infty_A} + \tfrac{1}{2}\rho V_{\infty_A}^2 = P_\infty + \tfrac{1}{2}\rho V_\infty^2, \tag{2.4}$$

and the continuity equation

$$h_{\infty_A} V_{\infty_A} = (h_B + h_F) V_\infty. \tag{2.5}$$

2.2. *Theoretical formulation*

As specified before, the aim of the problem is to define the function $z \mapsto w(z)$ and the geometry of the flow region in the physical plane by calculating the free streamlines CB and EF ($z = \int \mathrm{d}f/w$). This is usually done by conformal mapping of the potential plane (f-plane) and of the complex velocity plane (w-plane) onto an auxiliary plane (z-plane). As the region of variation in the f-plane is a strip of width $h_{\infty_A} V_{\infty_A}$ (figure 2), it is very easy to map. But when the walls are curved, the region of variation in the w-plane is unknown. So, rather than determining w, the problem is solved by determining the function Ω defined by

$$\Omega = -\mathrm{i}\log\left(\frac{V_{\infty_A}}{w}\right) = \Theta + \mathrm{i}T, \tag{2.6}$$

where Θ is the direction of the velocity V, and T is given by $|V| = V_{\infty_A} e^T$. T is constant on the two free streamlines CB and EF, and Θ is assumed to be determined by the shape of the walls (2.3). On the solid boundaries, we define β as the angle between the tangent at a given point and the x-axis, and s as the arclength starting from point C on the obstacle ($s \in [0; L_{Obs}]$), and from reference points I and J on the channel ($s \in] - \infty, +\infty[$). The solution to the problem then consists in solving a mixed-boundary problem for Ω (see §2.3 for greater detail). Indeed, the imaginary part of the function Ω is known on the fluid boundaries (free streamlines), and if the one-to-one correspondence ϵ between physical boundaries and those mapped onto the z-plane is assumed to be known, the real part of Ω on the solid boundaries (obstacle and channel) is known too. To solve this mixed problem, the physical plane is mapped inside a unit disk (figure 2), with the channel walls mapped onto the lower half-circle and the wetted wall of the obstacle onto an arc of the upper half-circle (point $\zeta = i$ corresponds to the dividing point D). The locations of points B, D, and F are fixed by conformal mapping of the ζ-plane onto the Z-plane, so we have to determine the locations of points A, C, and E. We will now establish the main equations of the theoretical method.

The Schwarz–Christoffel formula used to map the auxiliary Z-plane (figure 2) onto the f-plane is

$$f(Z) = K \int (Z - Z_B)^{-1} (Z - Z_D)(Z - Z_F)^{-1} \, \mathrm{d}Z$$

and this can be written

$$f(Z) = K \left[\frac{Z_B - Z_D}{Z_B - Z_F} \log(Z - Z_B) + \frac{Z_F - Z_D}{Z_F - Z_B} \log(Z - Z_F) \right] + \text{const.,}$$

where the value of the constant K has to be determined. By analysing $f(Z)$ in the vicinity of points B and F in the two planes considered, we obtain the following two equations, respectively:

$$K \frac{Z_B - Z_D}{Z_B - Z_F} = -\frac{h_B V_\infty}{\pi}, \quad K \frac{Z_F - Z_D}{Z_F - Z_B} = -\frac{h_F V_\infty}{\pi}. \tag{2.7}$$

Then, with (2.7) and the relation $f(Z_D) = 0$, the Schwarz–Christoffel formula is transformed into

$$f(Z) = -\frac{V_\infty}{\pi} \left[h_B \log\left(\frac{Z - Z_B}{Z_D - Z_B} \right) + h_F \log\left(\frac{Z - Z_F}{Z_D - Z_F} \right) \right] \tag{2.8}$$

with the additional relation from (2.7)

$$\frac{h_B}{h_F} = \frac{Z_B - Z_D}{Z_D - Z_F}. \tag{2.9}$$

The conformal mapping of the flow domain in the Z-plane onto the ζ-plane is defined by the correspondence of three pairs of points (we chose B, D and F here), and we have

$$\frac{(Z - Z_B)(Z_D - Z_F)}{(Z - Z_F)(Z_D - Z_B)} = \frac{(\zeta - 1)(i + 1)}{(\zeta + 1)(i - 1)},$$

which can be written with (2.9) as

$$Z = \frac{Z_B(h_F/h_B)(\zeta + 1) - iZ_F(\zeta - 1)}{(h_F/h_B)(\zeta + 1) - i(\zeta - 1)}. \tag{2.10}$$

Equation (2.10) can be written for point A ($Z_A = \infty$ on the Z-plane and $\zeta = e^{i\gamma_A}$ on the ζ-plane), to obtain a simple relation between γ_A and the two widths h_B and h_F. If we assume that the location of the two separation points C and E in the ζ-plane is known, corresponding to the affixes γ_C and γ_E, respectively, we can express Z_B and Z_F in terms of γ_A, γ_C, and γ_E with (2.10):

$$Z_B = \frac{\sin \frac{1}{2}(\gamma_C + \gamma_E)}{\sin \frac{1}{2}(\gamma_C - \gamma_E)} + \frac{2h_B \sin \frac{1}{2}\gamma_C \sin \frac{1}{2}\gamma_E}{h_F \sin \frac{1}{2}(\gamma_C - \gamma_E)}, \quad Z_F = \frac{\sin \frac{1}{2}(\gamma_C + \gamma_E)}{\sin \frac{1}{2}(\gamma_E - \gamma_C)} + \frac{2h_F \cos \frac{1}{2}\gamma_C \cos \frac{1}{2}\gamma_E}{h_B \sin \frac{1}{2}(\gamma_E - \gamma_C)}.$$

A new expression for the complex potential f can be written from these different equations for any point ζ of the flow domain in the ζ-plane, and its derivative is

$$\mathrm{d}f = \frac{-2h_{\infty_A} V_{\infty_A} \tan \frac{1}{2}\gamma_A (1 + i(\zeta - 1)/(\zeta + 1))}{\pi(1 - \tan \frac{1}{2}\gamma_A)(\zeta^2 - 1)(\tan \frac{1}{2}\gamma_A + i(\zeta - 1)/(\zeta + 1))} \mathrm{d}\zeta. \qquad (2.11)$$

If ζ corresponds to a point of the boundaries, we have then $\zeta = e^{i\sigma}$, and the expression for $\mathrm{d}f$ becomes

$$\mathrm{d}f = \frac{-2h_{\infty_A} V_{\infty_A} (1 - \tan \frac{1}{2}\sigma) \tan \frac{1}{2}\gamma_A}{\pi(1 - \tan \frac{1}{2}\gamma_A)(\tan \frac{1}{2}\gamma_A - \tan \frac{1}{2}\sigma) \sin \sigma} \mathrm{d}\sigma. \qquad (2.12)$$

As explained before, we will not determine the complex velocity w directly, but rather the Lévi–Civita function Ω (2.6). The reference velocity is taken at the upstream point A. We have $\zeta = e^{i\sigma}$ on the boundaries corresponding to the unit-circle, so we denote the functions θ and τ as $\theta(\sigma) = \Theta(e^{i\sigma})$ and $\tau(\sigma) = T(e^{i\sigma})$. On the solid boundaries, the real part of the Lévi–Civita function is then defined by

$$\theta(\sigma) = (\beta \circ \epsilon)(\sigma) - \pi \text{ if } \sigma \in [0; \pi/2[\quad \text{and} \quad \theta(\sigma) = (\beta \circ \epsilon)(\sigma) \text{ if } \sigma \in]\pi/2; 2\pi],$$

where ϵ is the one-to-one correspondence function between the boundaries AB, CDE, and FA in the ζ- and the z-planes.

The flow contains a singularity in the velocity field at the stagnation point D. This singularity is treated as usual (Gurevich 1966) by isolating the singular part of the function Ω, i.e. using $\Omega = \widetilde{\Omega} + \Omega_s$, where $\widetilde{\Omega}$ is a regular function and Ω_s a function having the same singularity as Ω. In this particular case, the singularity at the stagnation point consists in a jump of π for the function θ, and the velocity norm tends toward zero ($\tau \to -\infty$) at this point. So we have to find some function such as the following for satisfying these conditions:

$$\Omega_s(\zeta) = i \log(\zeta - i) = \theta_s(\sigma) + i\tau_s(\sigma).$$

We can thus say that

$$\theta_s(\sigma) = -\frac{\sigma}{2} + \begin{cases} \pi/4 & \text{if } \sigma \in [0; \pi/2[\\ 5\pi/4 & \text{if } \sigma \in]\pi/2; 2\pi], \end{cases} \qquad \tau_s(\sigma) = \ln \left| 2 \sin \frac{2\sigma - \pi}{4} \right|, \qquad (2.13)$$

and

$$\widetilde{\theta}(\sigma) = (\beta \circ \epsilon)(\sigma) + \frac{\sigma}{2} - \frac{5\pi}{4}, \quad e^{\widetilde{\tau}(\sigma)} = \frac{e^{\tau(\sigma)}}{2 \sin \frac{1}{4}(2\sigma - \pi)}. \qquad (2.14)$$

To solve the mixed boundary problem for the function $\widetilde{\Omega}$, we had to assume that the function $s \mapsto \beta(s)$ is known with the correspondence $\sigma \mapsto \epsilon(\sigma)$ on the solid boundaries, and the value of the function $\sigma \mapsto \tau(\sigma)$ on the free streamlines is given

by the relation

$$e^{\tau(\sigma)} = \frac{V_\infty}{V_{\infty_A}},$$

where V_∞ has to be determined.

It is then possible to define a new one-to-one correspondence ϵ with the relation

$$\epsilon(\sigma) = \int_{\sigma_{ref}}^{\sigma} ds = \int_{\sigma_{ref}}^{\sigma} |dz|, \tag{2.15}$$

where σ_{ref} is the affix of a reference point, and

$$dz = \frac{-h_{\infty_A} e^{i\theta(\sigma)} e^{\tilde{\tau}(\sigma)} (1 - \tan\frac{1}{2}\sigma) \tan\frac{1}{2}\gamma_A}{2\pi \sin\frac{1}{4}(2\sigma - \pi)(1 - \tan\frac{1}{2}\gamma_A)(\tan\frac{1}{2}\gamma_A - \tan\frac{1}{2}\sigma) \sin\sigma} d\sigma. \tag{2.16}$$

The location of the two separation points on the unit-circle can be found using the expression for the length of the wetted wall CDE:

$$L_{Obs} = \int_{\gamma_C}^{\gamma_E} |dz|. \tag{2.17}$$

When γ_C and γ_E are defined, it is also possible to determine the geometry of the two free streamlines CB and EF, and the values of h_B and h_F. For example, for the point E we have

$$z_F = z_E - \int_{\gamma_E}^{\pi} dz \tag{2.18}$$

and

$$h_F = \text{Im}\{z_F - z_E\}.$$

2.3. *Mixed-boundary problem*

As we have seen, in order to define the function $\sigma \mapsto \widetilde{\Omega}(\sigma)$ throughout the flow field, we have to solve a mixed-boundary problem on the unit disk of the ζ-plane. Let a flow domain be mapped onto the unit-disk such that the boundaries correspond to the unit-circle. This circle is divided into two parts: on the first (L'), we assume we know the real or imaginary part of the unknown function denoted ϕ. On the other part of the circle (L''), the other part of ϕ is known. This requires determining $2p$ zones on the circle ($L = L' \cup L''$). Using the notation of figure 3, we can say

$$L' = \bigcup_{i=1}^{p} b_i a_{i+1}, \quad L'' = \bigcup_{i=1}^{p} a_i b_i.$$

Solving the mixed-boundary problem then consists in determining the whole function ϕ, of which we know the real or the imaginary part, alternately, on the unit-circle. In the case of a domain corresponding to the unit disk, the solution of a Riemann–Hilbert problem implies that (Muskhelishvili 1977 and Weber 1999)

$$\phi(z) = \frac{X(z)}{i\pi} \int_L \frac{c(\sigma)}{[a(\sigma) + ib(\sigma)] X^+(\sigma)(\sigma - z)} d\sigma$$

with

$$a(\sigma) = 1, \quad b(\sigma) = 0, \quad c(\sigma) = \text{Re}\{\phi(\sigma)\} \text{ on } L',$$

$$a(\sigma) = 0, \quad b(\sigma) = -1, \quad c(\sigma) = \text{Im}\{\phi(\sigma)\} \text{ on } L'',$$
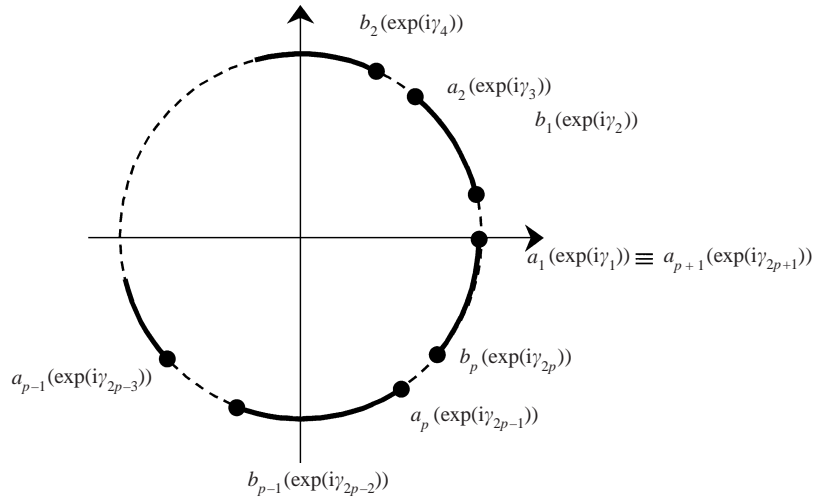
FIGURE 3. Mixed problem on a unit-circle.

and

$$X(\sigma) = \sqrt{\prod_{i=1}^{p}(z - a_i)(z - b_i)} \quad \left(X^+(\sigma) = X(\sigma) \text{ inside the disk}\right).$$

This expression exists provided the necessary and sufficient conditions are met for the existence of a solution vanishing at infinity:

$$\int_L \frac{\sigma^k c(\sigma)}{[a(\sigma) + ib(\sigma)] X^+(\sigma)} d\sigma = 0.$$

These equations yield

$$\phi(\sigma) = -\frac{\sqrt{\prod_{k=1}^{2p}\left|\sin\frac{1}{2}(\alpha - \gamma_k)\right|}}{2\pi}(-i)^{l+1}\sum_{j=1}^{p}\left[(-1)^j\left(I_{2j-1} + I_{2j}\right)\right] \qquad (2.19)$$

with

$$I_n = \int_{\gamma_n}^{\gamma_{n+1}} \frac{c(\sigma)\cos\frac{1}{2}(1-p)(\alpha - \sigma)}{\sqrt{\prod_{k=1}^{2p}\left|\sin\frac{1}{2}(\sigma - \gamma_k)\right|\sin\frac{1}{2}(\sigma - \alpha)}} d\sigma$$

where $\sigma \mapsto c(\sigma)$ represents the known part of the function ϕ and the $(p-1)$ equations for the necessary and sufficient conditions

$$\sum_{j=1}^{p}(-1)^j\left(C_{2j-1} + C_{2j}\right) = 0, \quad \sum_{j=1}^{p}(-1)^j\left(S_{2j-1} + S_{2j}\right) = 0 \qquad (2.20)$$

with

$$C_n = \int_{\gamma_n}^{\gamma_{n+1}} \frac{\cos[(\frac{1}{2}p - k)\sigma]c(\sigma)}{\sqrt{\prod_{k=1}^{2p}\left|\sin\frac{1}{2}(\sigma - \gamma_k)\right|}} d\sigma, \quad S_n = \int_{\gamma_n}^{\gamma_{n+1}} \frac{\sin[(\frac{1}{2}p - k)\sigma]c(\sigma)}{\sqrt{\prod_{k=1}^{2p}\left|\sin\frac{1}{2}(\sigma - \gamma_k)\right|}} d\sigma$$

where $k \in \left[1; p/2\right]$ if p is even, and $k \in \left[1; (p-1)/2\right]$ if p is odd. In the present

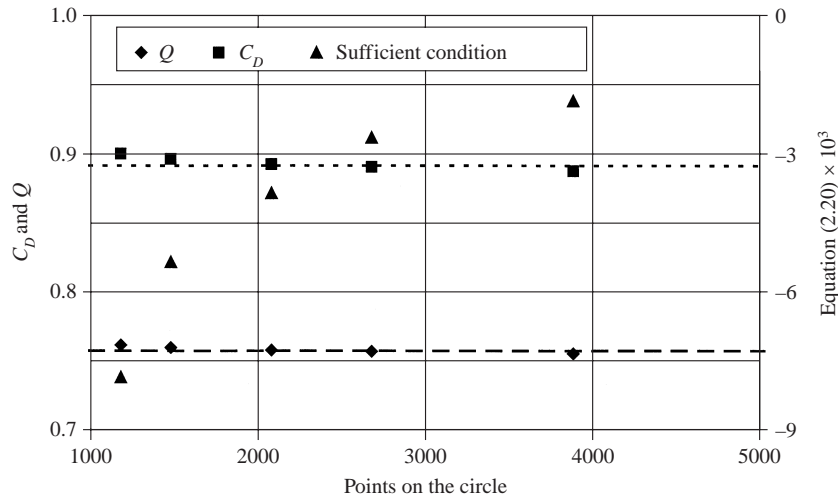FIGURE 4. Influence of the mean circle discretization step. The flow configuration is a arc of a cylinder ($2\Phi = 57°09'$ and $d = 2$) on the centreline of a plane channel ($h_{\infty_A} = 16.778$). The dotted lines correspond to the values given by Gurevich (see §2.5).

problem, p is equal to 2, so there is only one equation for the necessary and sufficient condition.

2.4. *Numerical solution*

The unknowns of the problem are the functions $\sigma \mapsto \widetilde{\theta}(\sigma)$, $\widetilde{\tau}(\sigma)$ and $\epsilon(\sigma)$, the widths h_B and h_F, the velocity V_∞ and the pressure P_∞ of the flow at the exit of the channel, and the location of points A, C and E on the unit-circle of the ζ-plane. The solution is obtained by solving the system of equations (2.5) and (2.13) to (2.20) using a recursive weighting scheme. We will now describe the initialization and one of these iterations in detail.

Initialization

The problem is defined by the geometry of the solid walls in Cartesian coordinates, the velocity V_{∞_A}, and the pressure P_{∞_A}. We can also initialize the velocity V_∞ at V_{∞_A}. The initial value for the angles γ_A, γ_C and γ_E is chosen at the beginning of the process: γ_A is commonly set at $270°$; the other two are chosen so as to yield faster results for the convergence of the whole scheme and when the flow is symmetrical, they are usually set to $\gamma_C + \gamma_E = 180°$. We must also initialize the first one-to-one correspondence $\sigma \mapsto \epsilon_0(\sigma)$ between the boundaries. The discretization on the circle is regular on the different zones, except in the vicinity of points A, B, and F corresponding to points at infinity, where a geometrical progression is assumed, to approach better infinity. Figure 4 shows the influence of the mean circle discretization step on the values of the drag coefficient C_D and the cavitation number Q (see §2.5, equations (2.21) and (2.22)), and on the result of equation (2.20) corresponding to the necessary and sufficient condition (the ideal value is 0). The other parameters (the number of points in the geometrical progression, the number of points in the solution to the mixed-boundary problem, initial values, and so forth) are identical. An acceptable average number of points seems to be around 2600, because more points will require more computation time but the results would be no better. Other parameters (such

as initialization or solution of the mixed problem) could be adjusted to reduce the value of the necessary and sufficient condition to about 10^{-6}.

Main iteration

(i) After initialization, the values of the functions $\sigma \mapsto \widetilde{\theta}(\sigma)$ and $\sigma \mapsto \widetilde{\tau}(\sigma)$ are determined by (2.14).

(ii) The mixed-boundary problem is solved in order to define the function $\widetilde{\Omega}$ in the flow field (2.19). We should point out that the ζ-plane discretization for this particular calculation is independent of the one used to solve the iterative process. For better results, the mean discretization step on the circle for the mixed problem is taken at $0.1°$. A finer discretization in the vicinity of the singular points is also useful.

(iii) Solving the mixed problem implies that the function $\widetilde{\tau}$ is known on the walls of the channel ($\sigma \in [\pi; 2\pi]$). By definition, at point A, we have the relation $\tau(\gamma_A) = 0$. We obtain a new value for the angle γ_A from the function $\tau = \widetilde{\tau} + \tau_s$, computed with (2.13) and (2.14) (the minimum or maximum of the function is taken because the function is equal to zero at several points before convergence). The discretization on the half unit-circle corresponding to the channel is then changed in such a way that the number of points on each side of A and the values of these functions $\widetilde{\theta}$ and $\widetilde{\tau}$ do not change (i.e. make a fan).

(iv) With the new value of γ_A, a new location is simultaneously found on the circle for the points C and E. To do this, the element ds is integrated over the arc of a circle CDE, changing the values of γ_C and γ_E with a fan to obtain the best value for the length of the wetted wall L_{Obs} (2.17). In order to know how to change the relative position of the two points, we use the necessary and sufficient condition of the mixed problem (2.20). The value of the equation corresponding to this condition is reduced in norms between two consecutive secondary iterations. The tolerance at convergence on this condition is very small (less than 10^{-6}).

(v) Once the locations of points C and E are defined, the geometry of the free streamlines CB and EF can be determined, along with the values of h_B and h_F (2.18).

(vi) In order to be able to repeat the iterative process, it is then useful to determine a new correspondence ϵ between the real and mapped boundaries using (2.15) and the computed values of γ_A, γ_C, and γ_E. The reference point on the wetted wall CDE is the point C. On the two infinite walls of the channel, the physical position of some reference points (I and J) first have to be defined. The location of these points is fixed in the f-plane (figure 2), and calculated in the ζ-plane using (2.8) and (2.10). The position of these points on the physical walls is found by interpolating their computed affixes in the preceding one-to-one correspondence. A new function ϵ can then be defined. To ensure better convergence of the recursive process, a weighting coefficient r is applied to the function ϵ. For the iteration number n, this can be written

$$\epsilon_n(\sigma) = (1 - r)\epsilon_n(\sigma) + r\epsilon_{n-1}(\sigma);$$

r is approximately 0.9.

(vii) The end of an iteration consists in the determination of the velocity on the free streamlines in accordance with the continuity equation (2.5) so that new values for the function τ can be defined.

The recursive scheme is reiterated until convergence, i.e. until the values for γ_A, γ_C, and γ_E are constant. At convergence (about 100 iterations) the entire flow field is defined and the lift and drag coefficients can then be determined.
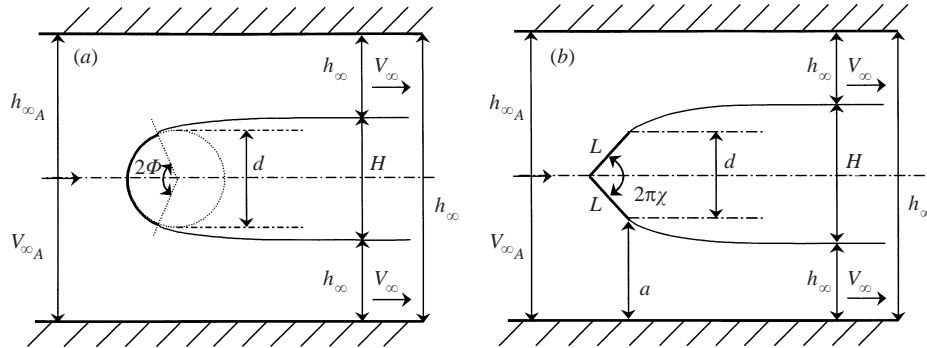
FIGURE 5. Analytical configurations studied in the literature: (*a*) arc of a cylinder and (*b*) symmetrical wedge.

2.5. *Analytical results*

We will first of all compare our computed results for particular flow configurations which have been treated analytically in the literature. Examples of such analyses can be found in Birkhoff & Zarantonello (1957) and Gurevich (1966). The walls of the channel are always considered to be planar and horizontal. The configurations discussed by these authors are the flow around a circular cylinder (for which the position of the separation points is defined) or a symmetrical flow around a wedge (a plate perpendicular to the flow direction is one special case of such flows).

Cylinder

Let us take a circular cylinder placed on the centreline of a plane channel. Birkhoff & Zarantonello and Gurevich used the Brillouin condition (see Jacob 1959, for example) to define the location of the separation points on the cylinder, so that the angle 2Φ defined by the wetted wall (arc CDE, with the notation of figure 1) is around $110°$–$120°$ for different values of V_{∞_A} (figure 5*a*). The drag coefficient C_D is usually defined by dividing the drag (obtained using the theorem of change of momentum in a planar channel of finite height h_{∞_A} and Bernoulli's equation; the pressure P_∞ is constant on the channel exit section) by $0.5\rho d V_{\infty_A}^2$:

$$C_D = \frac{h_{\infty_A}}{d}\left(\frac{V_\infty}{V_{\infty_A}} - 1\right)^2, \tag{2.21}$$

and the cavitation number Q by

$$Q = \left(\frac{V_\infty}{V_{\infty_A}}\right)^2 - 1. \tag{2.22}$$

In a finite planar channel with the above definition of the cavitation number Q, it should be noted that Q tends to 0 only in the case of cusped cavities ($V_{\infty_A} = V_\infty$). When the two plane walls are placed at infinity (tending toward ordinary Helmholtz flows), the method for setting up equation (2.21) is no longer valid.

Figure 6 compares the analytical results with our computations. Good agreement can be seen between the different cases despite the small differences for the high cavitation number that occur when the ratio between the width of the channel and the diameter of the cylinder is small. This could be explained by the small arc of circle in the ζ-plane corresponding to the free streamlines CB and EF, where the results are
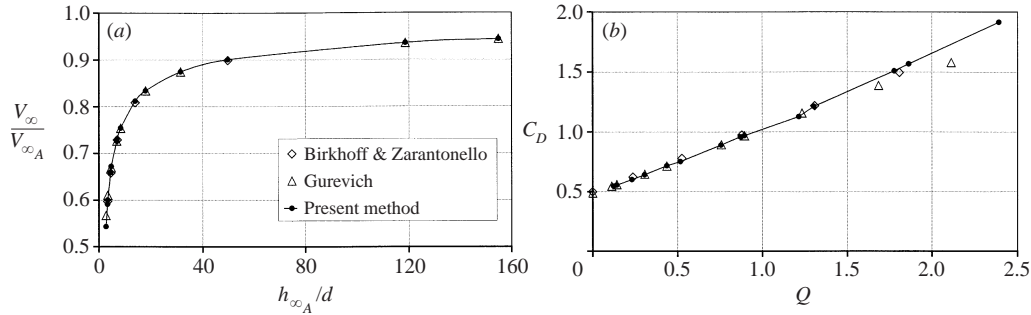
FIGURE 6. Comparison between analytical and computed results for the case of an arc of a circle placed between two infinite plates.

limited by the computed limits. We should note that the points given by the previous authors for $Q = 0$ must have been obtained with the usual Helmholtz flow hypothesis (with no channel, or with the walls at infinity) because the drag coefficient found is not zero ($C_D \approx 0.5$).

Moreover, it is well known that the Brillouin condition has no physical meaning, so we had to use experimental data obtained by PIV in order to get a realistic flow configuration (see §4).

Symmetrical wedge

The other flow configuration studied in the literature is the case of a symmetrical wedge (the interior angle being equal to $2\pi\chi$) on the centreline of a plane channel (figure 5b). The length of the wedge is $2L$. Of course, in this flow configuration, the separation points are located at the end of the wedge, so their positions are not indeterminate. For the purposes of Gurevich (1966), this problem is reduced by symmetry to analysis of the upper half of the flow region, while the stagnation line is considered to be a rigid wall. For $\chi = 1/2$, we have the flow around a flat plate placed perpendicularly to the flow. Gurevich gives the expression of the drag coefficient in this case as

$$C_D = \frac{1}{1 - 2a/h_{\infty_A}} \left(\frac{h_{\infty_A}}{2ak_a} - 1 \right)^2,$$

where the values of k_a for different ratios $2a/h_{\infty_A}$ and values of χ are given. The length of the wedge is taken to be equal to $2L = 2$, and the corresponding results are presented in figure 7. The expressions for the cavitation number (2.22) and the drag coefficient (2.21) are similar here, with the length d corresponding to the height of the wedge ($d = 2\sin(\pi\chi)$) in place of the cylinder diameter. As in figure 6, it can be seen in figure 7 that the ratio between the channel width and the plate height greatly affects the drag coefficient. The numerical and the analytical results are very similar. Again, the quality of the results declines as the arcs of circle corresponding to CB and EF decrease.

The good correspondence between these analytical results and our computed data implies that our numerical method appears to be validated for a great many symmetrical flow configurations. Since the configurations we can compute are more general than these however, we need experimental data to validate the corresponding results.
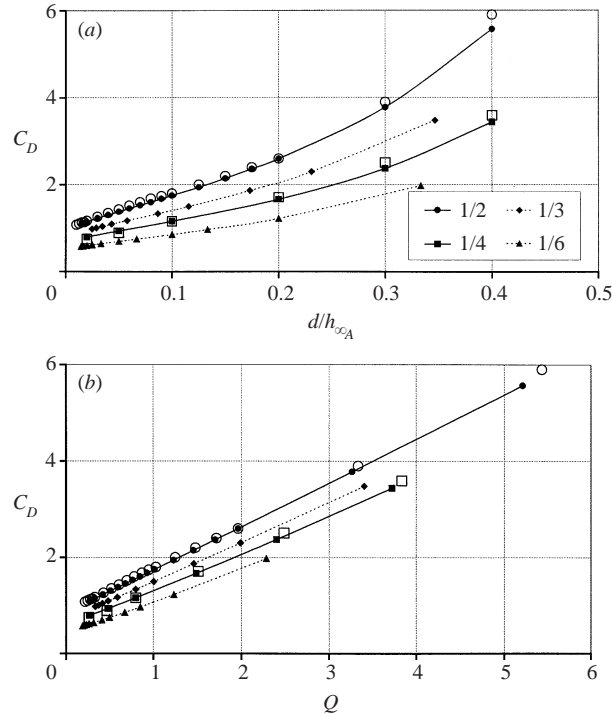
FIGURE 7. Numerical data for different symmetrical wedges: $\chi = 1/2$ (plate), $1/3$, $1/4$, and $1/6$ (in solid symbols) and analytical results (Gurevich 1966) for $\chi = 1/2$ and $1/4$ (in open symbols).

3. Experimental setup

3.1. *Wind tunnel*

All the experiments to test our numerical method were performed in an Eiffel wind tunnel. This is a subsonic open circuit wind tunnel. The section is square ($0.3\,\text{m} \times 0.3\,\text{m}$) and its length is $0.8\,\text{m}$ (figure 8). The maximum velocity generated by the electrically powered fan in the test section without an obstacle is $80\,\text{m s}^{-1}$. The obstacle is secured to the vertical walls of the wind tunnel. One of these walls is transparent, for direct visualization, and the laser sheet enters the wind tunnel section through a glass window in the floor.

3.2. *Particle image velocimetry (PIV) system*

The experimental data generated are the two-dimensional components of the velocity around the obstacle. In most PIV applications, the flow is seeded with tracer particles. In our case, an oil generator is used to generate and supply particles (the oil is vaporized on an electric resistor). The mean diameter of the particles is about $1\,\mu\text{m}$. The tracer particle generator is placed just in front of the honeycomb at the beginning of the wind tunnel convergent section. The laser sheet is generated by a double-oscillator laser. Here, we used a Nd/Yag laser (Spectra Physics 400) adjusted on the second harmonic and emitting two pulses of $200\,\text{mJ}$ each ($\lambda = 532\,\text{nm}$), at a repetition rate of $10\,\text{Hz}$. The laser sheet is developed with the usual laser sheet optics, with mirrors and spherical and cylindrical lenses with negative or positive focal length. To avoid overcrowding, an optical arm containing the mirrors is used and lenses allowed us to obtain a laser sheet with a divergence of about $60°$ and
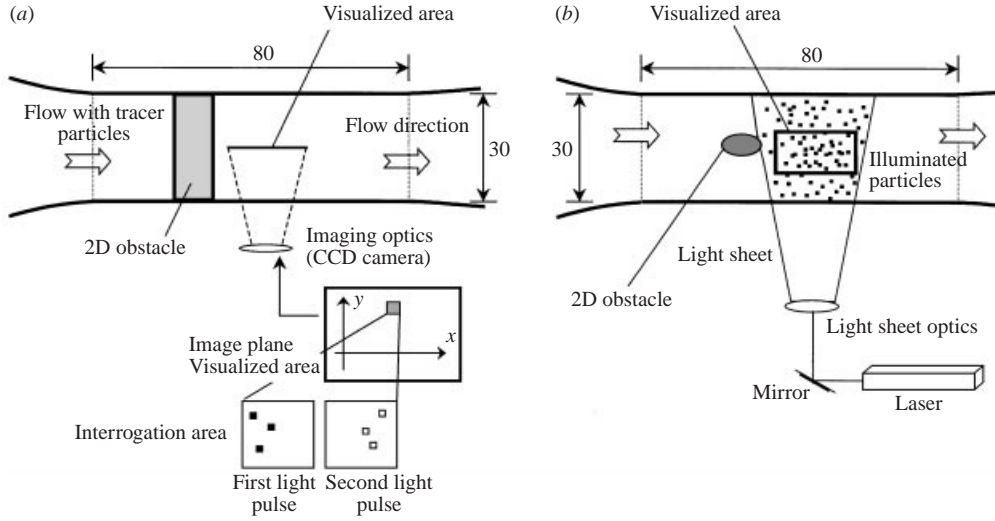
FIGURE 8. Wind tunnel section and experimental setup: (*a*) top view, and (*b*) front view. Dimensions in mm.

with a thickness of about 1 mm around the obstacle. For the experimental data that we present here, the flow images are picked up by a CCD with 1008×1016 sensor elements (camera CCD PIVCAM), placed perpendicularly to the laser sheet and in the direction of a section of the two-dimensional obstacle (figure 8). The laser pulses are synchronized with the image acquisition by a TSI synchronizer system driven by InSight-NT^{TM} software. For all the results presented in this paper, the PIV recordings are divided into small subareas (interrogation areas) corresponding to 32×32 pixels. For data post-processing, the interrogation areas overlap by 50%, which corresponds to defining 61×62 vectors on the visualized area. The local displacement vector is determined for each interrogation area by statistical methods (auto-correlation). The projection of the local flow velocity vector onto the laser sheet plane is calculated by *InSight* using the time delay between the two illuminations (Δt) and the magnification at imaging. The post-processing used here is very simple – merely a velocity range filter.

4. Results

We will now test the performance of our numerical method by comparing our computed results with experimental data for more general cases than those treated in the literature. But first, we will again consider the symmetrical configuration of a circular cylinder placed in a plane channel.

4.1. *Cylinder*

As mentioned before, the results presented by Birkhoff & Zarantonello and Gurevich do not represent physical flow configurations. Indeed, the values taken for the separation points on the cylinder are very small (Brillouin's condition) and not realistic.

The diameters d of the different cylinders studied are 50, 80 and 120 mm. The velocity at the channel entry is varied in order to move the position of the separation point. The flow is defined by the Reynolds number $Re = V_{\infty_A} d/\nu$. Figure 9 represents a velocity field obtained by PIV for one of the configurations studied: the cylinder
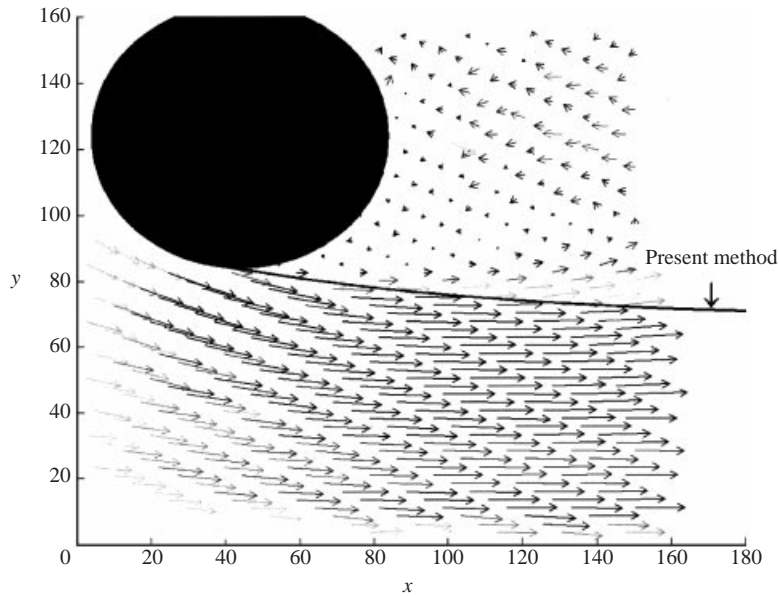
FIGURE 9. Velocity field and computed free streamline for $d = 80$ mm and $Re = 56\,000$. $\Phi = 85°$.

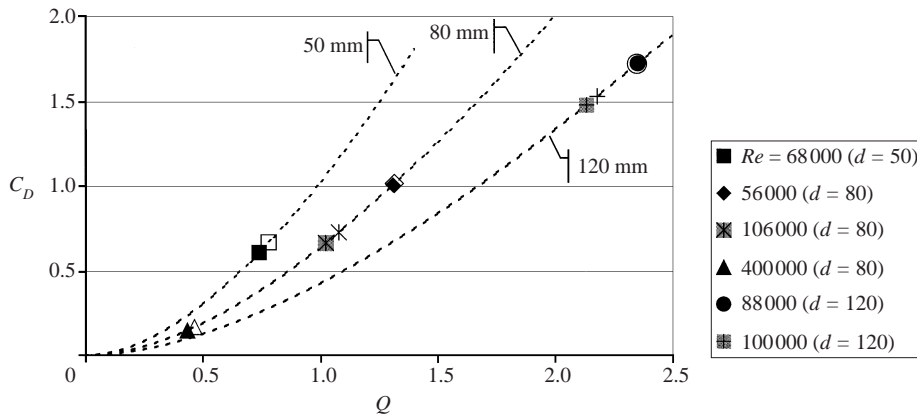FIGURE 10. Variation of the drag coefficient C_D with the cavitation number Q. Comparison between experimental (filled) and computed (hollow) data for different Reynolds numbers and cylinder diameters.

diameter is 80 mm and the Reynolds number 56 000. The interrogation area of the flow field measures 2.5×2.5 mm here, and the time delay Δt is set at 30 μs. Experiments give the separation angle Φ as 85°. We superimposed the computed free streamline geometry on the velocity field, and find a good correspondence between experimental and computed data for the wake geometry behind the cylinder. Equivalent results were obtained for the free streamline geometry for the other diameters and other Reynolds numbers, and so for other separation angles (from 80° to 100°).

With the experimental data, it is also possible to evaluate the velocity V_∞ behind the cylinder. Of course, physically, the wake behind the cylinder is closed (indeed, we can see recirculation areas in the PIV velocity fields), unlike the model used numerically. We also note that the free streamlines on the PIV velocity fields are almost horizontal
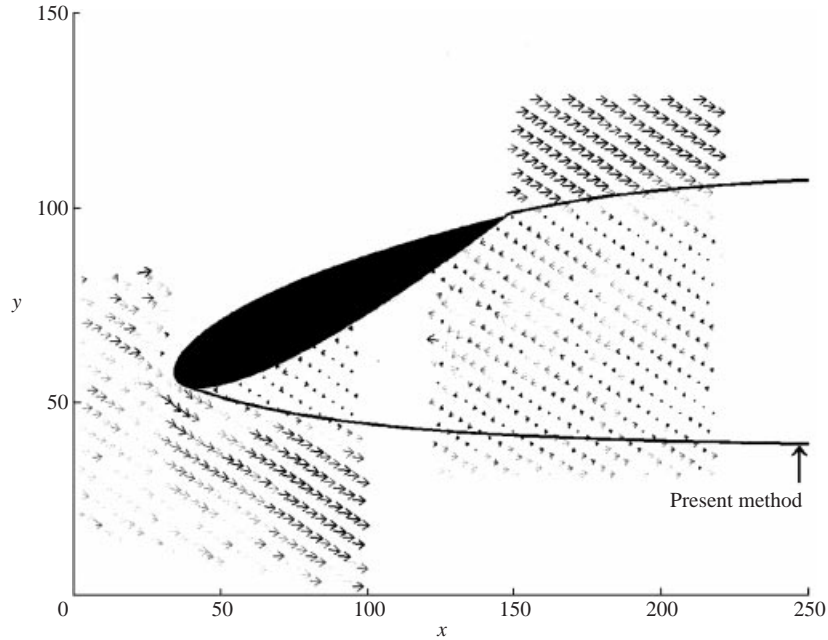
FIGURE 11. Experimental velocity fields obtained by PIV and computed streamline in an asymmetrical configuration: NACA0015 profile with incidence $-20°$ and $Re = 210\,000$.

beyond one diameter behind the cylinder. The velocity V_∞ can thus be evaluated from the experimental data. Figure 10 shows the variation of the drag coefficient C_D with the cavitation number Q, using the experimental velocities V_{∞_A} and V_∞, and equations (2.21) and (2.22). These two equations can be related, yielding

$$C_D = \frac{h_{\infty_A}}{d} \left(\sqrt{Q+1} - 1 \right)^2.$$

This function is drawn on figure 10 for the three ratios h_{∞_A}/d studied (6, 3.75, and 2.5). We can see good correspondence between the different results (experimental and computed), despite the simplicity of the model of the wake we used. Also, the drag coefficient decreases as the separation angle Φ increases, for the three configurations with the cylinder of diameter 80 mm. It was previously pointed out that, in order to have $Q \to 0$ in a finite plane channel, the cavity has to be cusped. That is, as the Reynolds number increases, the separation angle Φ increases too, and there is a tendency toward the configuration of a cusped flow. This is the reason why there is a very small value of C_D for the Reynolds number of 400 000.

4.2. *Asymmetrical configuration*

These asymmetrical flow configurations (asymmetrical obstacles or channels) have not been studied in the literature.

Asymmetrical obstacle

The first asymmetrical obstacle we studied experimentally was a NACA0015 profile at an incidence of $-20°$. The chord c of the profile is 120 mm. The chord-referenced Reynolds number chosen is 210 000. Again, the PIV velocity field is used to validate the computed data. Two velocity fields are used to determine the geometry of the two
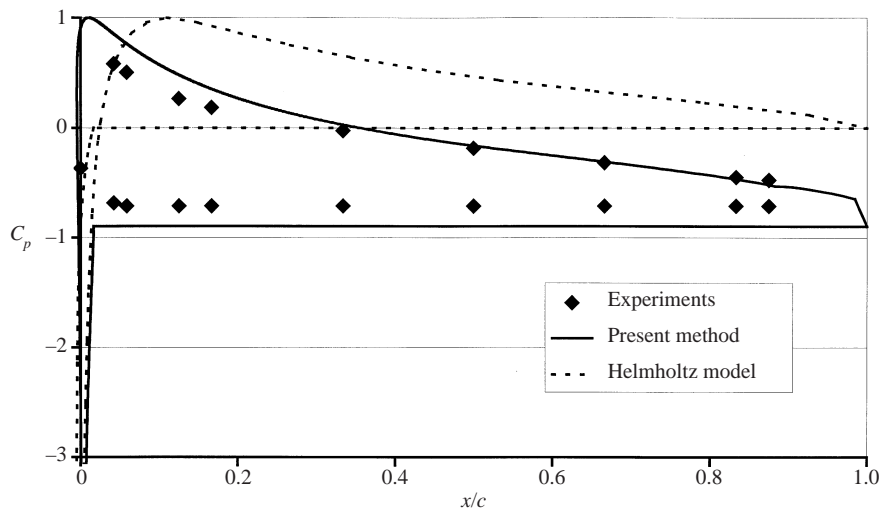
FIGURE 12. Variation of the pressure coefficient along the chord for the NACA0015 profile.

free streamlines. The PIV parameters are a visualization area of 95×95 mm and a delay of 5 μs between two pulses. Here again, good agreement can be seen between the computed streamline and the experimental velocity field (figure 11). The profile was instrumented with a number of pressure sensors along the chord. Figure 12 shows the variation of the pressure coefficient along the profile. The computations for the profile in an infinite stream with the Helmholtz model are plotted too, to bring out the effect of the walls. It is well known that the Helmholtz model is not very realistic, but it can still be seen that, when the obstacle is placed in a channel, the pressure coefficient in the wake is evaluated better with our numerical method even considering the very simple model of the Helmholtz wake.

Another example of a general configuration is the flow around a symmetrical obstacle (a circular cylinder) bounded by two plane walls, placed off the channel centreline. The experimental data presented here correspond to a cylinder of diameter 80 mm, displaced 30 mm up in the channel, with a Reynolds number of 120 000. The separation points are not symmetrical in this case: they are at 80° on the top side and 85° underneath. Again, two velocity fields are used to determine the whole flow field. The dimensions of the interrogation areas are 120×120 mm and the time delay 5 μs. The results are presented in figure 13. It can be seen that the relative positions of the free streamlines for the Helmholtz problem (infinite stream) and the flow bounded by walls are closer for the greatest separation angle. The small difference (5°) in the separation angles on the obstacle greatly affect the geometry of the free streamlines.

Asymmetrical channel

For this third asymmetrical flow configuration, we performed no experiments as this proved difficult in practice. The good results for the other configurations, however, strongly hint that the same would be true here. We investigated an obstacle (which may or may not be symmetrical) placed between two arbitrary walls. Figure 14 gives the shape of the free streamlines in the case of an arc of an ellipse placed in an asymmetrical channel. We should point out that the equations for the walls are given here, not because they are needed to solve the numerical problem (as might be the case with other numerical methods), but so as to create the walls more easily. Note
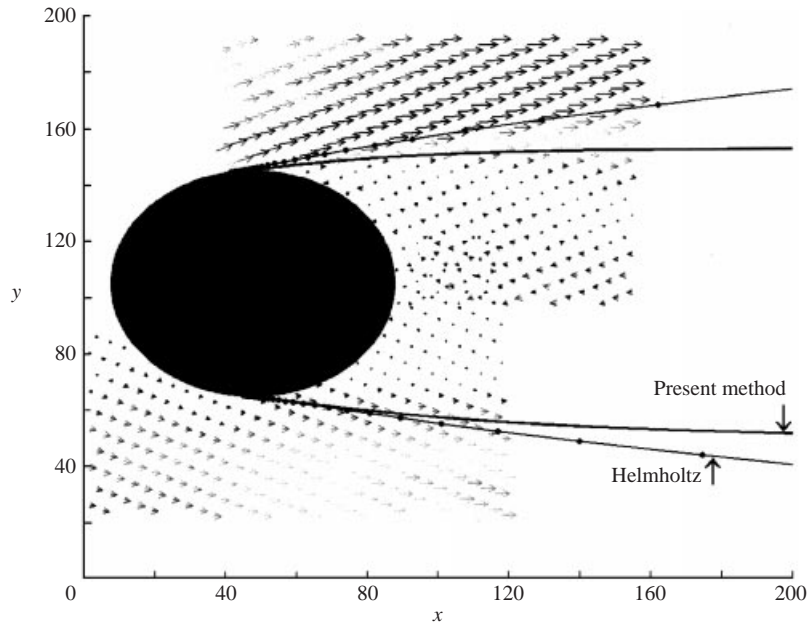
FIGURE 13. Experimental velocity fields obtained by PIV and computed streamlines in an asymmetrical configuration: cylinder (diameter 80 mm) shifted from the centreline of the channel by 30 mm and for $Re = 120\,000$.
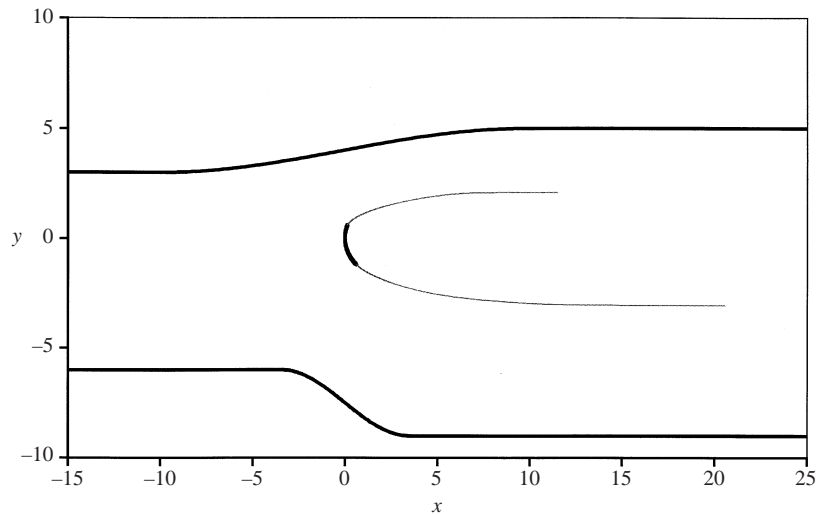

FIGURE 14. Free streamlines geometry in the case of an asymmetrical configuration. The shape of the obstacle is given by $x = 3 - \sqrt{1 - y^2/4}$ for $-1.2 \leqslant y < 0.6$, the upper wall by $y = 3$ for $x < -10$, $y = \sin(\pi x/20) + 4$ for $|x| < 10$; and $|y| = 4$ for $x > 10$; and the lower wall by $y = -6$ for $x < -3.5$, $y = -1.5 \sin(\pi x/7) - 7.5$ for $|x| < 3.5$, and $y = -9$ for $x > 3.5$.

that expression (2.21) is not valid for a non-planar channel. For the case presented in figure 14, we found $V_\infty = V_{\infty_A} \approx 1.016$, and consequently $Q \approx 0.03$ from (2.22). When the drag coefficient is determined by integrating the pressure coefficients over the obstacle, the value is 0.11. So there must exist a flow configuration in a non-planar

channel configuration with a cavitation number equal to zero ($V_\infty = V_{\infty_A}$) and with a drag coefficient other than zero on the obstacle, without having a cusped cavity as for flow in a finite plane channel.

5. Conclusion

The numerical method presented, based on complex potential theory, solves the problem of determining the flow field over a two-dimensional obstacle placed in an arbitrary channel and using the Helmholtz wake model. This problem was solved in order to see if our numerical method is suitable for a prediction of the flow around the obstacle and its wake and of the pressure distribution on the obstacle, i.e. its drag and lift. Of course, our main assumption is that the fluid is ideal, and the unsteady problem in the wake is not taken into account. Solving this problem implies solving a mixed-boundary problem with four zones on the unit-circle, the main consequence of which is that more computation time is required because of the accuracy needed to solve this particular problem. The numerical method is based on the solution of a recursive scheme involving the different unknowns, and convergence is reached for about 100 iterations with good accuracy. It takes around 2 hours computation time on a PC Pentium 300 MHz computer.

The numerical method has been validated twice: first, by comparison with the analytical results published in the literature (simple symmetrical flow configurations with a planar channel), and then with different experimental data obtained in more general configurations. We have found close agreement between experimental data and analytical results (for the flow around the circular cylinder), and more generally among all the data, both in symmetrical and asymmetrical configurations.

These experiments were useful in validating our computations, but also in determining the physical position of the separation points on the cylinder. We have seen that these positions have to be known in order for the numerical method to work, and that their position greatly affects the wake geometry and the different forces. As the general method seemed to give good results on comparison with experimental data, it might be useful to couple it with a boundary layer model in order to predict the position of the separation points. This has been done for an obstacle in a free stream with the Helmholtz model (Legallais & Hureau 1994). This method can be used here, so the flow field and the different forces on the obstacle can be determined with no experimental data, for any kind of obstacle, and any channel geometry.

REFERENCES

BIRKHOFF, G. & ZARANTONELLO, E. H. 1957 *Jets, Wakes and Cavities*. Academic Press.

BLOOR, M. I. G. 1978 Large amplitude surface waves. *J. Fluid Mech.* **84**, 167–179.

CISOTTI, U. 1911 *Rend. Accad. Lincei.* **30**(5), 314–502.

DIAS, F. & ELCRAT, A. R. 1992 Ideal jet flow with a stagnation streamline. *Eur. J. Mech. B/Fluids* **11**, 233–247.

DIAS, F. & TUCK, E. O. 1991 Weir flows and waterfalls. *J. Fluid Mech.* **230**, 525–539.

EFROS, D. 1946 Hydrodynamical theory of two-dimensional flow with cavitation. *Dokl. Akad. Nauk SSSR* **51**, 267–270.

ELCRAT, A. R. & TREFETHEN, L. N. 1986 Classical free-streamline flow over a polygonal obstacle. *J. Comput. Appl. Maths* **14**, 251–265.

EPPLER, R. 1954 Beiträge zu Theorie und Auwendung der unstetigen Strömungen. *J. Rat. Mech. Anal.* **3**, 591–644.

FORBES, L. K. & SCHWARZ, L. W. 1982 Free-surface flow over a semi-circular obstruction. *J. Fluid Mech.* **114**, 299–314.

GUREVICH, M. I. 1966 *Theory of Jets in an Ideal Fluid*. Pergamon Press.

HANNA, S. N., ABDEL-MALEK, M. N. & ABD-EL-MALEK, M. B. 1996 Super-critical free-surface flow over a trapezoidal obstacle. *J. Comput. Appl. Maths* **66**, 279–291.

HUREAU, J., BRUNON, E. & LEGALLAIS, PH. 1996 Ideal free streamline flow over a curved obstacle. *J. Comput. Appl. Maths* **72**, 193–214.

HUREAU, J. & WEBER, R. 1998 Impinging free jets of ideal fluid. *J. Fluid Mech.* **372**, 357–374.

JACOB, C. 1959 *Introduction Mathématique à la Mécanique des Fluides*, Gauthier-Villars.

KING, A. C. & BLOOR, M. I. G. 1987 Free-surface flow over a step. *J. Fluid Mech.* **182**, 197–208.

KING, A. C. & BLOOR, M. I. G. 1990 Free-surface flow of a stream obstructed by an arbitrary bed topography. *Q. J. Mech. Appl. Maths* **43**, 87–106.

LEGALLAIS, PH. & HUREAU, J. 1994 Singularity method applied to the classical Helmholtz flow coupling procedure with boundary layer calculation. *J. Phys.* III, *Paris* **4**, 1053–1068.

LEGALLAIS, PH., HUREAU, J. & BRUNON, E. 1995 Determination of flows past curved obstacles with wakes using a mixed problem solution. *Eur. J. Mech* B/*Fluids* **14**, 275–299.

MILNE-THOMSON, L. M. 1968 *Theoretical Hydrodynamics*, 5th Edn. Macmillan.

MUSKHELISHVILI, N. I. 1977 *Singular Integral Equations*, 5th Edn. Noordhoff International Publishing.

PENG, W. & PARKER, D. F. 1997 An ideal fluid jet impinging on an uneven wall. *J. Fluid Mech.* **333**, 231–255.

RIABOUCHINSKY, D. 1921 On steady fluid motion with free surface. *Proc. Lond. Math. Soc.* **2**(19), 206–215.

ROSKHO, A. 1954 *A new hodograph for free streamline flow theory. NACA TN* 3168.

TOISON, F. & HUREAU, J. 2000 Open-channel flows and waterfalls. *Eur. J. Mech* B/*Fluids* **19**, 269–283.

VANDEN-BROECK, J.-M. & KELLER, J. B. 1982 Jets rising and falling under gravity. *J. Fluid Mech.* **124**, 335–345.

WEBER, R. 1999 Modélisation d'écoulements bidimensionnels de fluide parfait. Application aux jets et sillages épais (profils rigides ou déformables) avec validation expérimentale. PhD thesis, Université Orléans.

WEBER, R., LEROY A., TOISON, F. & LOYER, S. 1999 Étude de sillages épais dans un écoulement 2D: confrontation de résultats numériques et expérimentaux (PIV – anémométrie à fil chaud). *14ème Congrès Français de Mécanique. Toulouse.*

WU, T. Y. & WANG, D. P. 1964 A wake model for free streamline flow theory. *J. Fluid Mech.* **18**, 65–93.